FREQUENCY CHARACTERIZATION OF A MAGNETICALLY ACTUATED MEMS RESONANT BIOSENSOR

V. Russino, F. Pieri
Dipartimento di Ingegneria dell'Informazione, Università di Pisa, Via G. Caruso 16, 56122 Pisa, Italy

D. Paci
STMicroelectronics, Via Tolomeo 1, 20010 Cornaredo, Italy

Keywords: Biosensors, Resonant sensors, Microbalances, MEMS.

Abstract: In this work, the mass response of a resonant, CMOS (Complementary MOS) compatible MEMS sensor, oriented at the detection of diagnostic markers, is presented. The sensor is fabricated with a MEMS (Micro-electro-mechanical System) post-processing method on a standard, CMOS-based VLSI technology, retaining maximum compatibility with the CMOS process flow. The mechanical resonator is based on inductive actuation and detection, and the sensing is based on the microbalance principle. A protocol for covalent bonding of organo-functional silanes (to be used as link sites for biomolecular probes) on the resonator surface is presented. The effect on the mechanical frequency response of a test mass attached to the surface is demonstrated by grafting of gold nanoparticles (NP's) to the amino-terminated surface silanes.

1 INTRODUCTION

MEMS resonators have been proposed as biosensors based on the gravimetric principle, trying to transfer the approach of the ubiquitous Quartz Crystal Microbalance (QCM) to the MEMS domain. Miniaturization of resonant biosensors could lead to several advantages: reduced amount of biological samples, possibility of integration of multiple sensors on a single substrate (sensor arrays), potential for the integration of conditioning electronics on the same chip, with consequent improved SNR and, in turn, sensitivity. While the fabrication of piezoelectric MEMS resonant sensors (the microscopic counterpart of the QCM) is certainly possible (Zuniga et al., 2009), other transduction mechanisms are accessible in the MEMS world: for example capacitive (Teva et al., 2006), piezoresistive (Sone et al., 2004), each with advantages and drawbacks.

A few specific issues must be addressed in the design of a feasible MEMS resonant biosensor: the device (and its package) must withstand operation in a liquid environment (a severe requirement, for example, in capacitive MEMS resonators which are prone to stiction, i.e. elastocapillary collapse (Maboudian and Howe, 1997); the functionalization protocol of the resonator surface must be compatible with other on-chip components (metal lines used for electric signal distribution, on-board electronics, etc.) (Lenci et al., 2010). In this work, we addressed these issues by developing a MEMS torsional resonator with magnetic driving and sensing.

The high torsional stiffness and large cavity under the moving parts eliminates the stiction problem, while a carefully designed silanization protocol allows for reliable operation of the sensor. In the following, after a description of the design, MEMS fabrication and functionalization methods, we present a full electrical characterization of the resonators in terms of its frequency response.

The operation of the resonator as a microbalance is demonstrated by anchoring gold NP's on the resonator surface and measuring the consequent shift in resonance frequency. A discussion of the experimental data is then carried out, and an estimate of the sensor mass sensitivity is presented.

2 DESIGN AND FABRICATION

The proposed MEMS sensor is based on a torsional resonator, whose overall structure is sketched in Fig.1

Russino V., Pieri F. and Paci D..
FREQUENCY CHARACTERIZATION OF A MAGNETICALLY ACTUATED MEMS RESONANT BIOSENSOR.
DOI: 10.5220/0003167803910396
In *Proceedings of the International Conference on Biomedical Electronics and Devices* (BIODEVICES-2011), pages 391-396
ISBN: 978-989-8425-37-9

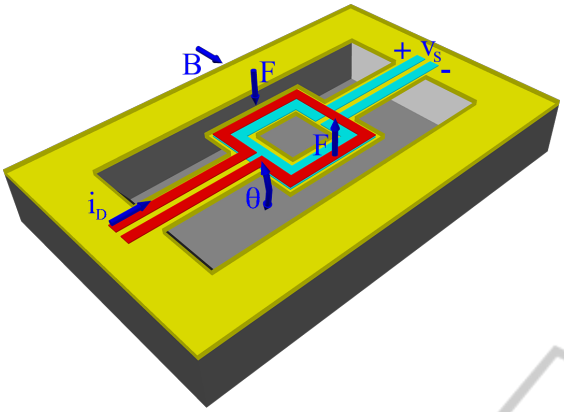

Figure 1: Sketch of the sensor structure.

(Paci et al., 2008). A square plate with a central hole (the hole is required for fabrication purposes, see section 2.2) is suspended over a cavity etched on a crystalline silicon substrate by means of two thin beams, acting as torsional springs. Two separate, concentric inductors (in red and light blue in Fig.1) are embedded in the plate, while the electrical connections to the inductors are embedded in the suspending beams.

To drive the plate into mechanical resonance, an external static magnetic field (provided, for example, by a permanent magnet) is required. An alternating current injected in one of the inductors (the *driving loop*) generates Lorentz forces on two sides of the loop, and the resulting mechanical torque drives the plate into oscillation, whose amplitude is only significant (a few degrees at its maximum) if the frequency of the driving signal is close to or exactly at the mechanical resonance frequency of the structure.

Because of the external magnetic field, an EMF (electromotive force) at the same frequency of the input current is induced on the second inductor (the *sensing loop*). The amplitude of this EMF is significant only at the resonance frequency, so that the device effectively acts as a frequency selective system (a resonant filter). A parasitic voltage component, caused by mutual inductance between the two inductors, is also present at the output.

The surface of the plate is biochemically activated by covalent bonding of an organo-functional silane layer, with a protocol which retains CMOS compatibility with other on-board components (including electronic circuits). The functional group of the silane molecule can be used to link bioreceptors, which in turn bind specifically with the target biomolecule. The resulting shift in mass can be measured by the consequent shift in the resonance frequency with an all-electrical measurement system. It this work, gold nanoparticles (NP's) (Diegoli et al., 2006) anchored to amino terminal groups of the silane molecules were used as the test mass to demonstrate the viability of the transduction mechanism.

2.1 Magneto-mechanical Modelling

Despite being a distributed parameter system, the device depicted in Fig.1 can be described with reasonable accuracy by a reduced model by treating it as a lumped parameter mechanical resonator, governed by an ordinary differential equation:

$$J\ddot{\theta} + D\dot{\theta} + k\theta = \Gamma_D i_D(t) \tag{1}$$

where θ is the rotation angle of the plate, J is its the rotational moment of inertia, D is a damping coefficient (mostly caused by viscous losses in the surrounding air), k is a torsional spring constant, Γ_D is the input magneto-mechanical coupling coefficient (proportional to the external magnetic field) (Tilmans, 1996), and i_D is the driving current.

The mechanical resonance frequency f of the system is thus $f_0 = 1/2\pi \cdot \sqrt{k/J}$. Theoretical and simulated resonance frequencies for our devices are in the $25 \div 100\,\mathrm{kHz}$ range. A straightforward analysis shows that in presence of an additional surface mass density μ_S (caused by the analyte captured at the plate surface), the resonance frequency undergoes a relative shift equal to:

$$\frac{\Delta f}{f_0} = -\frac{1}{2}\frac{\mu_S}{t_P \rho_P} \tag{2}$$

where t_P and ρ_P are the plate thickness and volume mass density, respectively.

From the electrical point of view, a complete equivalent two-port network can be developed for the device (Paci et al., 2008). Its open circuit trans-admittance (output voltage to input current transfer function) is equal to:

$$H(s) = \left.\frac{V_S(s)}{I_D(s)}\right|_{I_S=0} = \frac{\frac{\Gamma_D \Gamma_S}{k}}{1 + \frac{s^2}{\omega_0^2} + \frac{s}{Q\omega_0}} + Ms \tag{3}$$

where Γ_D and Γ_S are input and output magneto-mechanical coupling coefficients, $\omega_0 = 2\pi f_0$ is the resonance angular frequency, $Q = \sqrt{kJ}/D$ is the resonator quality factor, M is the mutual inductance between the two loops, and s is the generalized (complex) angular frequency.

2.2 Device Fabrication

The devices process fabrication is based on the post-processing of the STMicroelectronics BCD6s process. The resonator plate is fabricated from the

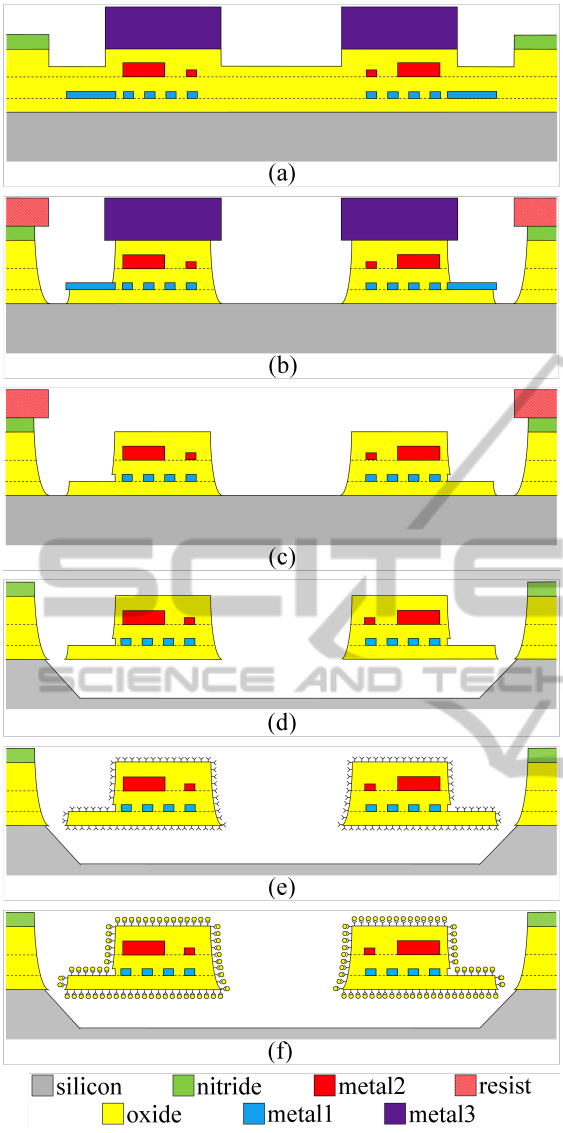

Figure 2: Sketch of the MEMS fabrication process (not to scale). The single steps are described in the text.

inter-metal dielectric layers, while loops are fabricated using the metal interconnection layers. A post-processing sequence, designed to be CMOS compatible, was used to release the microbalance.

The silicon chip section as received from the foundry is shown in Fig.2a. The thick metal3 layer (dark purple) is used as a mask to protect the resonator structure during the subsequent etch of the dielectrics, basically silicon dioxide (yellow), while the external structures (connection lines from and to the loops, pads, etc.) are protected by a standard photolithographic resist (pink). The oxide is removed in a buffered HF solution (Fig.2b) to reach the silicon substrate surface. At this point, the metal3 is not

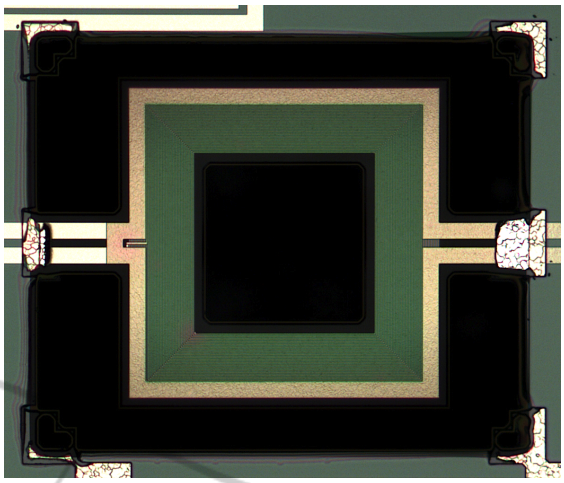

Figure 3: Optical microscope photograph of one the fabricated resonators. The plate side length is 400 µm. The driving loop (yellow outer border) is clearly visible. The dark area corresponds to the cavity in the silicon substrate.

required anymore and is then removed in a wet etch (Fig.2c). The resist is removed as well, and the release phase can be performed. During the release, carried out in a buffered tetra-methyl-ammonium hydroxide (TMAH) solution at 85 °C, the silicon under the plate is anisotropically etched along (100) planes, so that the plate and springs are mechanically detached from the substrate. The chemistry of the TMAH solution is tuned to allow etch of the silicon while removing both the oxide and the metal negligibly (Biswas et al., 2006). Because of the anisotropy, a central hole is required in the plate to allow complete release of the structure (Fig.2d). At this point, the resonators appear as in Fig.3. The overall dimensions of a resonator is (depending on the specific type) in the range of a few hundreds of micrometers.

Once the mechanical structure of the resonator is ready, the sample is glued to the final, gold plated ceramic package which will be used for electrical characterization, and the silanization phase takes place. Organo-functional silane deposition is commonly used as an intermediate step towards the creation of bioactive protein layers in biosensing applications. In this work, the silanization protocol developed in (Lenci et al., 2010) was tailored to suit the needs of the specific application.

A preliminary cleaning of the sample in an ammonia based solution ($NH_4OH(25\%)$:H_2O:$H_2O_2(30\%)$ 1:1:4 vol.) is performed. After 5′ in the solution, the sample is rinsed twice in deionized water (D.I.). After this step, the resonator surface is terminated by hydroxyl groups, which are required to allow covalent bonding of the silane. While sulphuric acid-based solutions (e.g. piranha) are most commonly used in the

literature (Kim et al., 2008), they are not compatible with exposed aluminium which is present in our samples at the external electric pads.

Immediately after rinsing, the sample is immersed in an aqueous solution of 3-amino-propyl-triethoxysilane (APTES) (0.05% vol.) for 5′, and rinsed again in D.I. (Fig.2e). The sample then undergoes a curing phase (Ballarin et al., 2008) by immersion in acetone for 60′. During this phase, loosely bound silane molecules or silane clusters are removed and the overall quality of the silane layer improves.

At this point, the resonators are ready for characterization. A single silicon chip contains up to four resonators. The input and output inductors of each resonator are bonded to the package gold contacts by means of thin aluminum wires (Fig.4). A first frequency response of the resonator is measured using the procedure detailed in the next section. To eliminate the influence of ambient humidity (a common interferer for gravimetric sensor), the sample is heated in oven at 120 °C for 30′ and immediately moved to a sealed aluminium box for the electrical characterization. The resonators are then loaded with an additional mass to verify their behaviour as gravimetric sensor.

The added mass is represented by gold NP's which are known to bind to the exposed amino groups of the silane layer. A 25 µl drop of a 30 nm gold NP colloid (British Biocell International) is deposed on the chip (Fig.2f). After 60′, the sample is rinsed in D.I., dried in oven (30′ at 120 °C), and the frequency response of the resonators is then measured again. To ensure that the NP anchoring is specific to the silane layer, a reference sample underwent the same procedure with the exclusion of the silanization steps.

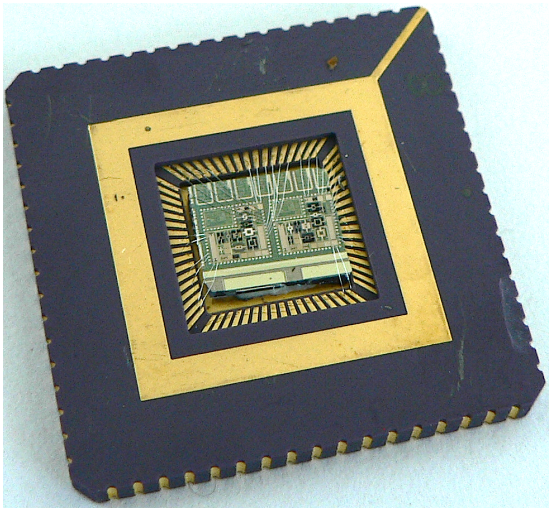

Figure 4: Photograph of a sensor chip mounted in its ceramic package. Each chip contains four working resonators. The bonding wires connecting the chip pads to the package are also visible. The package side is 2.5 cm.

The amount of added mass was estimated by Scanning Electron Microscope (SEM) observation of the resonator front surface at several different test sites (6 to 8 for each resonator). The number of NP's at each site, 1 µm × 1 µm in size, was counted and averaged. The resultant added mass density μ_S was calculated by supposing a constant diameter of 30 nm for each NP, and then multiplied by the total resonator surface to obtain an estimate of the total added mass. No trace of NP's was found on the reference sample.

3 CHARACTERIZATION SETUP

The instrumentation setup for electrical characterization is sketched in Fig.5. The input current is provided by a waveform generator. The output voltage signal is pre-amplified (the voltage level is in the hundreds of microvolt range) and then fed to a lock-in amplifier, which measures the amplitude and phase relationship between the input and the output signal. Both the waveform generator and amplifier are remotely controlled by a personal computer.

The external magnetic field is provided by two permanent magnets. The field amplitude is around 70 mT. Before each measurement session, the sample is dried in oven (see section 2.2) and placed in a sealed aluminium box. At least two measurement sessions are performed for each resonator: one after silanization, and one after NP grafting.

For each session, four different frequency curves are measured: the first, with a 20 kHz measurement window centred at the theoretical resonance frequency, obtained by FEM (Finite Element Method) simulations, is used to identify the actual resonance frequency peak. The other three measurements are performed around the actual resonance frequency with a 500 Hz window and a 5 Hz step. Each curve requires between 10 and 30 minutes.

Moreover, as the magneto-mechanical coupling coefficients (Γ_D and Γ_S of Eq.3) are proportional to the magnetic field, a single response curve without

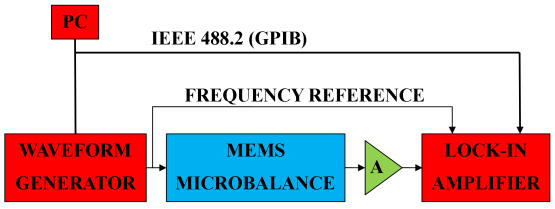

Figure 5: Schematic representation of the experimental setup for electrical characterization.

Table 1: Experimentally extracted parameters for two different resonators.

MB108	f_0 [Hz]	σ_{f_0} [Hz]	f_D [Hz]	σ_{f_D} [Hz]	Q	σ_Q	μ_S [kg/m^2]	σ_{μ_S} [kg/m^2]	S [m^2/kg]
200×200	94581	2.5	94291	2.5	287	1.26	$3.67\cdot10^{-5}$	$0.57\cdot10^{-5}$	−79.59
400×400	31749	1.0	31612	0.6	157	5.67	$3.86\cdot10^{-5}$	$1.31\cdot10^{-5}$	−117.27

magnets (and thus with $\Gamma_D = \Gamma_S = 0$) is also performed on each resonator to extract the value of the mutual inductive coupling coefficient M.

The purely mechanical response (i.e. the first term in the RHS of Eq.3) is then extracted by subtraction of the mutual inductance term from the actual measured data. The obtained data points are then numerically fitted against the analytical expression of the mechanical response to extract the most relevant mechanical parameters, most importantly (from the application point of view) the resonance frequency f and the quality factor Q. For each resonator, their values are averaged over the three measurements. Typical measured response curves are presented in Fig.6, where the effect of the added mass on the resonance frequency is also shown.

4 DISCUSSION AND CONCLUSIONS

Typical extracted parameters from two different resonator types, fabricated on the same chip, are summarized in Table 1. The MB108-400 resonator is the device shown in Fig.3; the MB108-200 resonator is a similar device, but with a smaller central plate (200 µm × 200 µm) and comparatively longer suspension springs. For each parameter, both the averaged value (over three measures) and its standard deviation (σ_*) are shown.

The initial resonance frequency f_0 was measured immediately after silanization, and its value is affected by very little error. The resonance frequency after NP exposure, f_D is consistently lower than the initial frequency, and corresponds to a frequency shift of a few hundred hertz (or 0.75% and 0.30% for the two resonators, respectively). While the resonance frequency tends to drift to higher values after a few days on ambient storage (most likely because of adsorption of ambient moisture), a drying step (30′ at 120 °C) recovers its original value almost completely.

The frequency shifts must be compared to the measured values of the added mass density μ_S to obtain an estimate of the sensor sensitivity. Given the different area of the two devices, a sensitivity parameter allowing a fair comparison can be defined as (Janshoff et al., 2000):

$$S = \frac{\frac{f_D - f_0}{f_0}}{\mu_S} [\mathrm{m^2 kg^{-1}}] \quad (4)$$

The measured values for our resonators are around 79.6 and 117.3 m^{2}kg^{-1} for the two devices (Table 1, last column). These values compare favourably to the typical values for macroscopic QCM's (about 1 m^{2}kg^{-1} in (Janshoff et al., 2000)), but also to other MEMS resonant sensors: (Zuniga et al., 2009), for example, claims about 60 m^{2}kg^{-1}. Compare also, for a review, (Shen et al., 2010).

If the resonator plate thickness and density are known, Eq.2 can be used to extract a theoretical value of the mass density $\mu_{S,T}$ from experimental frequency shift data. If this analysis is carried out for our devices, the theoretical mass density is consistently higher than the measured one (by a factor of two or more in some cases), with a correspondingly higher value of the actual sensitivity S. Separate FEM analysis confirms the trend implied by the simplified analytical model used to obtain Eq.2, so that this discrepancy cannot attributed to oversimplification in the mechanical model. Several other factors might come into play in this case. Among them, the effect of the NP adhesion on the residual (usually compressive) stresses of the plate oxide film (which are certainly present due to fabrication issues and were neglected in this analysis) and on the overall stiffness of the mem-

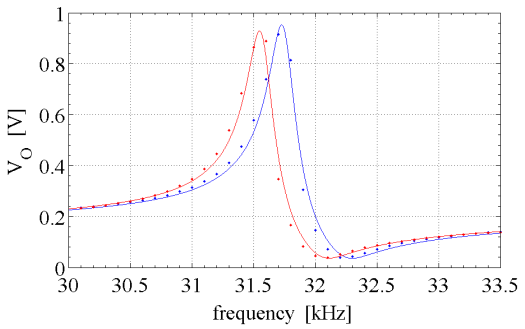

Figure 6: Frequency response of the resonator of Fig.3, before (blue) and after (red) NP grafting. Actual data are indicated by the dots, while the lines are fitted curves. The contribution of the mutual inductance is not subtracted yet (see text).

brane (in particular in the torsional beams).

In conclusion, we demonstrated the operation of a magnetically actuated MEMS resonator with electrical input and output as a sensitive mass sensor. The measured sensitivities can be compared favourably to standard QCM's and other implemented MEMS microbalances. Moreover, a MEMS-compatible silanization protocol for the resonator active surface was developed as well. Such a silane layer can be used as a precursor to the fabrication of a bioactive layer to transform the device in a complete resonant biosensor.

ACKNOWLEDGEMENTS

This work was partly financed under a PRIN 2008 grant by the Italian Ministry for University and Research.

REFERENCES

Ballarin, B., Cassani, M., Scavetta, E., and Tonelli, D. (2008). Self-assembled gold nanoparticles modified ito electrodes: The monolayer binder molecule effect. *Electrochim. Acta*, 53:8034–8044.

Biswas, K., Das, S., Maurya, D., Kal, S., and Lahiri, S. (2006). Bulk micromachining of silicon in tmah-based etchants for aluminum passivation and smooth surface. *Microel. J.*, 37:321–327.

Diegoli, S., Mendes, P., Baguley, E., Leigh, S., Iqbal, P., Diaz, Y. G., Begum, S., Critchley, K., Hammond, G., Evans, S., Attwood, D., Jones, I., and Preece, J. (2006). ph-dependent gold nanoparticle self-organization on functionalized si/sio2 surfaces. *Journal of Experimental Nanoscience*, 3:333–353.

Janshoff, A., Galla, H., and Steinem, C. (2000). Piezoelectric mass-sensing devices as biosensors - an alternative to optical biosensors? *Angew. Chem. Int.*, 39:4004–4032.

Kim, J., Seidler, P., Fill, C., and Wan, S. (2008). Investigations of the effect of curing conditions on the structure and stability of amino-functionalized organic films on silicon substrates by fourier transform infrared spectroscopy, ellipsometry, and fluorescence microscopy. *Surf. Sci.*, 602:3323–3330.

Lenci, S., Tedeschi, L., Domenici, C., Lande, C., Nannini, A., Pennelli, G., Pieri, F., and Severi, S. (2010). Protein patterning on polycrystalline silicon–germanium via standard uv lithography for biomems applications. *Materials Science and Engineering C*, doi:10.1016/j.msec.2010.07.002.

Maboudian, R. and Howe, T. (1997). Critical review: adhesion in surface micromechanical structures. *J. Vac. Sci. Technol. B.*, 15:1–20.

Paci, D., Pieri, F., Toscano, P., and Nannini, A. (2008). A cmos-compatible, magnetically actuated resonator for mass sensing applications. *Sensors and Actuators B*, 129:10–17.

Shen, W., Mathison, L., Petrenko, V., and Chin, B. (2010). A pulse system for spectrum analysis of magnetoelastic biosensors. *Appl. Phys. Lett.*, 96:163502.

Sone, H., Okano, H., and Hosaka, S. (2004). Picogram mass sensor using piezoresistive cantilever for biosensor. *Jpn. J. Appl. Phys.*, 43:4663–4666.

Teva, J., Abadala, G., Torresa, F., Verda, J., Pérez-Murano, F., and Barniola, N. (2006). A femtogram resolution mass sensor platform, based on soi electrostatically driven resonant cantilever. part i: Electromechanical model and parameter extraction. *Ultramicroscopy*, 106:800–807.

Tilmans, H. (1996). Equivalent circuit representation of electromechanical transducers: I. lumped-parameter systems. *J. Micromech. Microeng*, 6:157–176.

Zuniga, C., Rinaldi, M., Khamis, S., Johnson, A., and Piazza, G. (2009). Nanoenabled microelectromechanical sensor for volatile organic chemical detection. *Applied Physics Letters*, 94:223122.